A Multiswitch Open-Circuit Fault Diagnosis of Microgrid Inverter Based on Slidable Triangularization Processing

Zhanjun Huang and Zhanshan Wang, *Senior Member, IEEE*

***Abstract*—In this article, a robust inverter fault diagnosis algorithm is proposed under microgrid environment considering unbalanced state and overcurrent component interference. First, the detected signals are transformed into different data triangles by the proposed slidable triangularization processing which can conveniently and effectively extract the multiscale trend features and data jitter components. Further, the signed features are obtained by the proposed jitter signing processing method, which can reduce the influence of amplitude, and facilitate the logical operation and mixed operation. Then, a quantitative trend fault degree is calculated by the signed information to reflect the fault degree and location information, which has the characteristics of quantitative change. It can reduce the fluctuation and quantity of fault data features. Finally, echo state network is used to implement the intelligent classification. Because the design of hidden layer and the network training speed is simple and fast, which makes the design, implementation, and debugging of fault diagnosis more convenient. Compared with the existing fault diagnosis algorithms, it is robust to unbalanced state and overcurrent component interference of microgrid. These features make it more suitable for inverter fault diagnosis of microgrid environment. The effectiveness of fault diagnosis algorithm is verified by the experiments and comparisons.**

***Index Terms*—Fault diagnosis, features extraction, jitter signing processing (JSP), microgrid inverter, slidable triangularization processing (STP).**

I. Introduction

MICROGRID unit mainly includes dc sources, battery, inverter, inductance capacitance filter, transmission lines, and bus, as shown in Fig. 1. It can bring many practical advantages such as mitigation of peak demand, reducing emission, improving reliability, and power quality through appropriate control strategies [1], [2]. However, microgrid has many challenges [3]–[9], e.g., open-circuit fault diagnosis of microgrid inverter is one of them. Accurate open-circuit fault diagnosis approach is the key step for improving reliability of microgrid.

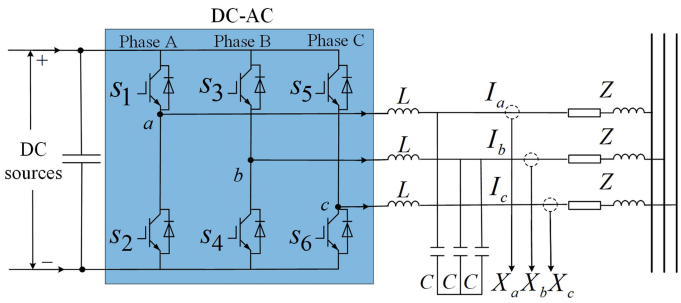

Fig. 1. Main structure of a microgrid inverter.

In recent years, the open-circuit fault diagnosis of inverter has been widely studied [10]–[19]. Wu *et al.* [10] proposes a $a-b$ trajectory method of open-circuit fault based on the mathematical models of three-phase balanced inverter system, which uses the difference from each other to realize the diagnosis. In [11], the distortion observer is obtained by the normal model analysis. Then, the estimated distortions are compared with the threshold value to determine the fault condition. An *et al.* [12] build a mixed logical dynamic model based on balanced state to estimate the error between the expected and the detected currents for fault diagnosis. Freire *et al.* [13] propose an instantaneous maximum value of the three-phase current absolute values as a new normalizing quantity under the assumption of a perfectly balanced three-phase sinusoidal current system, which can realize many kinds of fault diagnosis, like open-circuit fault and current sensor fault of inverter. Wu *et al*. [14] define Allelic Points to measure the symmetry of detected signal, and the main feature of asymmetry of fault data is used to diagnose the fault. In [15], the average absolute values are used as principal quantities to formulate the diagnostic variables to compare with the threshold of theory model under three-phase balanced condition. Zhao and Cheng [16] use the current Park's vector method to normalize the detected current signals, which are used to calculate the ratio of moving average and absolute moving average of phase currents as diagnostic variables. When failure occurs, the asymmetrical feature is effectively extracted. In [17],

Manuscript received February 11, 2020; revised May 26, 2020; accepted June 8, 2020. Date of publication June 25, 2020; date of current version September 4, 2020. This work was supported in part by the National Natural Science Foundation of China under Grants 61973030, 61433004, and 61627809, in part by the Liaoning Revitalization Talents Program under Grant XLYC1802010, and in part by SAPI Fundamental Research Funds under Grant 2018ZCX22. Recommended for publication by Associate Editor Prof. B. Mirafzal. *(Corresponding author: Zhanshan Wang.)*

Zhanjun Huang is with the State Key Laboratory of Synthetical Automation for Process Industries, College of Information Science and Engineering, Northeastern University, Shenyang 110819, China, and also with the College of Aeronautics, Northwestern Polytechnical University, Xian 710072, China (e-mail: zj_huang@sina.com).

Zhanshan Wang is with the State Key Laboratory of Synthetical Automation for Process Industries, College of Information Science and Engineering, Northeastern University, Shenyang 110819, China (e-mail: zhanshan_wang@163.com).

Color versions of one or more of the figures in this article are available online at https://ieeexplore.ieee.org.

Digital Object Identifier 10.1109/TPEL.2020.3004531

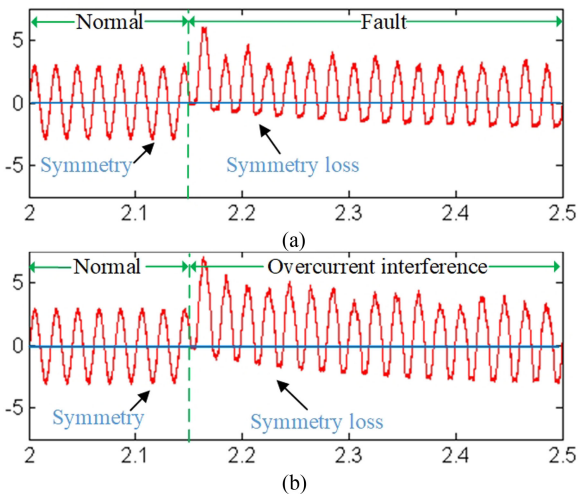

Fig. 2. Feature comparison of experimental results for s2 open-circuit fault state and overcurrent component interference. (a) s2 open-circuit fault state. (b) Overcurrent component interference.

the summation of currents with semiperiod phase-difference is used as diagnostic variables; then the normalized way based on the absolute phase currents and variable parameter moving average method are applied to improve the diagnostic speed. In [18], the current Luenberger observer model is implemented to estimate the current signals, which are used to compare the average and rms of the detected currents to extract fault component. In [19], a normalized phase current based on Park's transformation is used to calculate the average value; it reflects the symmetry feature of the detected signals.

Above methods in [10]–[19] show better performance for open-circuit fault diagnosis of inverter. However, when the related methods are applied to the fault diagnosis of microgrid inverter, there are still many practical problems, such as microgrid unbalanced state [20]–[22] and overcurrent component [23]–[25]. For unbalanced state of microgrid, it can cause the amplitude asynchronous and uncertain relationship of three-phase currents. In fact, many methods [10]–[16] are based on three-phase balanced state to analyze the model and obtain the related conclusions or threshold, e.g., the trajectory of two output currents is an ellipse in the cartesian coordination under assumption that three phases are balanced in [10], $\max|i_a|, |i_b|, |i_c| \approx I_m[\frac{\sqrt{3}}{2} + (1 - \frac{\sqrt{3}}{2})|\cos(3\omega t + \phi)|]$, $i_a + i_b + i_c = 0$, in [13], and so on. Hence, if they are used directly in unbalanced state of microgrid, which may cause some adverse effects.

On the other hand, the overcurrent component is the interference of inverter fault diagnosis. It emphasizes a kind of interference feature that the current of part phase increases sharply in a short time and leads to strong asymmetry, which is similar with the part features of the open-circuit fault of inverter. Fig. 2 shows the feature comparison of experiments for s2 open-circuit fault state and overcurrent component interference, respectively. In Fig. 2(a), it can be seen that when s2 open-circuit fault occurs, the current signal loses the symmetry feature. This feature is widely used for inverter switches fault diagnosis by various mathematical ways [15], [16], [17], [18], [19]. They are sensitive to asymmetric features. When open-circuit faults occur, their diagnosis variables show obvious changes which can effectively identify open-circuit faults. However, in Fig. 2(b), it can be seen that when overcurrent interference appears, the current signal also loses the symmetry feature, which is similar with open circuit. This similar feature may lead to uncertain fluctuations of fault diagnosis features and results, even false alarm for some diagnosis methods based on symmetry features. It can be seen from the above analysis, that there are many difficulties for inverter fault diagnosis in microgrid. Unbalanced state and overcurrent component of microgrid have seriously negative effects on inverter fault diagnosis, which would lead to the unavailability of many observer models and basic conclusions, and the difficulty in threshold selection and fault feature extraction.

Hence, in order to improve above problem, and make the fault diagnosis of inverter more suitable for microgrid environment, a robust multiswitch open-circuit fault diagnosis algorithm for microgrid inverter considering unbalanced state and overcurrent component interference is proposed in the article. The proposed algorithm mainly includes slidable triangularization processing (STP), jitter signing processing (JSP), the calculation of quantitative trend fault degree, and echo state network (ESN). Particularly, STP is mainly used to extract the multiscale trend features, data jitter components, and key points and reduce the startup times of diagnosis method by transforming the detected data curves into different data triangle. JSP is used to avoid the influence of amplitude and facilitate the calculation by signing multiscale trend feature and relative position information. The quantitative trend fault degree is calculated to reflect the degree of trend fault and fault position information. ESN is used to detect the type and the location of the inverter switch fault. The main contributions of this article are summarized as follows.

1) STP method is proposed which mainly uses the triangle to describe data curve and extract quantitative key features' information. It can extract multiscale trends of the divided curves, key points, and data jitter components conveniently and effectively. Meanwhile, because the fault diagnosis algorithm is driven by the slidable triangle, it can reduce the startup times and facilitate the corresponding calculation.
2) JSP method is proposed, which can sign the extracted key information by the jitter component. It can prevent key information from the influence of amplitude, and facilitate the logical operation and mixed operation.
3) A feature variable for quantitative trend fault degree is proposed, which has the characteristics of quantitative change. It can effectively reduce the fluctuation and quantity of fault data features. Meanwhile, only one variable contains trend fault degree and location information. It is conducive to the stability of diagnostic results. In addition, ESN is used together with this variable to make the design, training, implementation, and debugging of fault diagnosis more convenient.

This article mainly focuses on the research of fault diagnosis of inverter, which is important for microgrid. Compared with

the operation environment of motor drive systems, the operation environment of microgrid is more complex, and the unbalanced state and overcurrent component are more common, which have seriously negative effects on inverter fault diagnosis. Hence, the research object is the microgrid inverter in this article, which focuses on the robustness of the fault diagnosis against unbalanced state and overcurrent component interference of microgrid. In principle, the method is presented in the microgrid, but it can also be used for many other applications by further considering the other required features.

This article is organized as follows. The proposed fault diagnosis algorithm is described in Section II. Section III shows the experimental results. The conclusion is provided in Section IV.

II. Proposed Fault Diagnosis Algorithm

Through the above analysis, it can be understood that in order to improve the robustness to unbalanced state and overcurrent component interference, the proposed diagnosis algorithm need to avoid using the related features of symmetry, amplitude, component missing, and the model analysis of three-phase balanced state. Hence, it is necessary to solve this problem from other ways. First, the flowchart of function module for the proposed algorithm is given in Fig. 3. The proposed fault diagnosis algorithm mainly includes STP, JSP, quantitative trend fault degree, and ESN module.

The sampling model of detected signal is described as follows:

$$X_\phi(i) = I_\phi(i \cdot r) \tag{1}$$

where I_ϕ is the detected current signal, ϕ represents the different phases, X_ϕ refers the sampled discrete data, r is the sampling interval, and i is the sampling point. If the data can be virtually folded p times, the data will be divided into N_c' curves and N_p' fold points

$$N_c' = 2^p \tag{2}$$

$$N_p' = 2^p + 1. \tag{3}$$

The space of fold points Sp is obtained by

$$\text{Sp} = \left[\frac{N-1}{N_c'}\right] = \left[\frac{N-1}{2_p}\right] \tag{4}$$

where $[\cdot]$ is the integer processing. Further, the location $P_v^i(i')$ of any fold point i' can be represented as

$$P_v^i(i') = \left[\frac{(i'-1)N + 2^p \cdot i - i' + 1}{2^p}\right], i' \in [1, N_p']. \tag{5}$$

If each curve corresponds to a fold line, the end $P_e(i)$ of fold line starting with i is $P_v^i(2)$

$$P_e(i) = P_v^i(2) = \left[\frac{N + 2^p \cdot i - 1}{2^p}\right]. \tag{6}$$

The center value $\widehat{D}_\phi(i)$ for sampled data with i location can be obtained by average processing with $2L+1$ length

$$\widehat{D}_\phi(i) = \frac{1}{2L+1} \sum_{n=i-L}^{i+L} X_\phi(n). \tag{7}$$

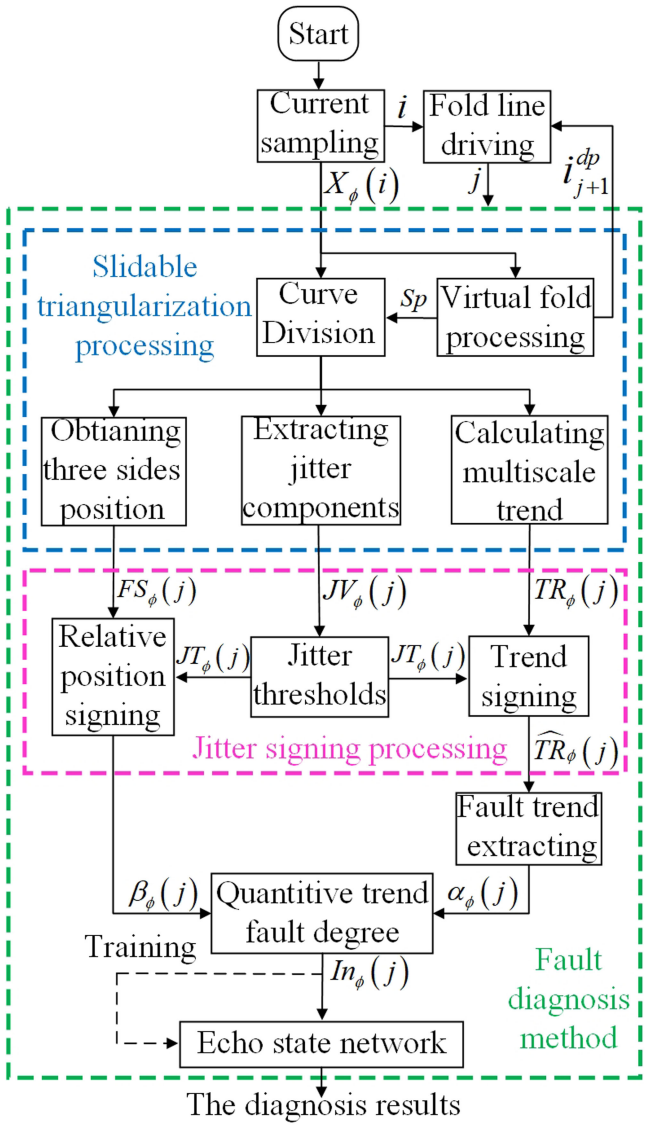

Fig. 3. Flowchart of function module for the proposed fault diagnosis algorithm.

Then, the fold line starting with i can be expressed as

$$F_\phi(i) : \left[(i, \widehat{D}_\phi(i)), (P_e(i), \widehat{D}_\phi(P_e(i)))\right]. \tag{8}$$

If two adjacent curves form a large curve, the fold line corresponding to this large curve ending with i can be expressed as

$$\text{BF}_\phi(i) : \left[(i - 2 \cdot \text{Sp}, \widehat{D}_\phi(i - 2 \cdot \text{Sp})), (i, \widehat{D}_\phi(i))\right]. \tag{9}$$

For jth fold line, the corresponding relationship of endpoints is

$$\begin{cases} i_j^E = i_j^F + \text{Sp} \\ i_j^F = i_{j-1}^E. \end{cases} \tag{10}$$

Then, the drive point of $j+1$th fold line is

$$i_{j+1}^{dp} = P_e(i_j^E) + L = \left[\frac{N + (i_j^E + L)2^p - 1}{2^p}\right]. \tag{11}$$

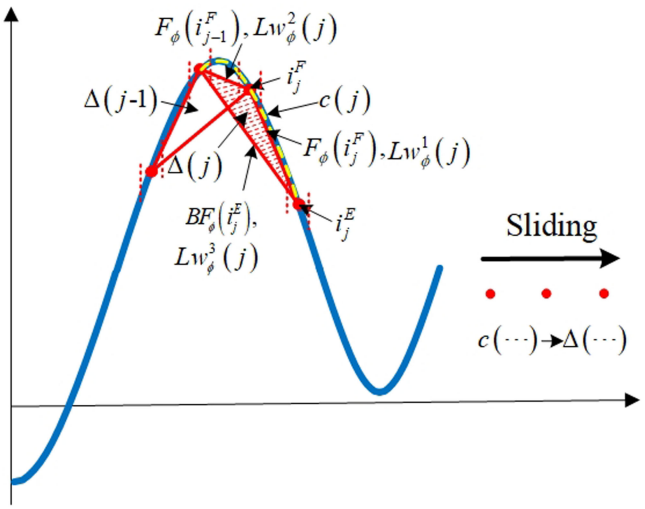

Fig. 4. Principle diagram of STP.

The big curve $c(j)$ is consisted of jth curve and nearest $j-1$th curve. As shown in Fig. 4, if each curve is replaced by a fold line, the big curve $c(j)$ can be replaced by a triangle $\triangle(j)$. The three sides of triangle $\triangle(j)$ can be expressed as

$$\mathrm{FS}_\phi(j):\left[F_\phi(i_j^F), F_\phi(i_{j-1}^F), \mathrm{BF}_\phi(i_j^E)\right]. \tag{12}$$

The coefficients $\mathrm{Lw}_\phi^1(j)$, $\mathrm{Lw}_\phi^2(j)$, $\mathrm{Lw}_\phi^3(j)$ of three sides represent the trend of corresponding fold lines $F_\phi(i_j^F)$, $F_\phi(i_{j-1}^F)$, $\mathrm{BF}_\phi(i_j^E)$, which can be obtained by

$$\begin{cases}\mathrm{Lw}_\phi^1(j)=\widehat{D}_\phi(P_e(i_j^F))-\widehat{D}_\phi(i_j^F)\\ \mathrm{Lw}_\phi^2(j)=\widehat{D}_\phi(P_e(i_{j-1}^F))-\widehat{D}_\phi(i_{j-1}^F)\\ \mathrm{Lw}_\phi^3(j)=\widehat{D}_\phi(i_j^E)-\widehat{D}_\phi(i_j^E-2\cdot\mathrm{Sp}).\end{cases} \tag{13}$$

The obtained multiscale trends $\mathrm{TR}_\phi(j)$ is described as

$$\mathrm{TR}_\phi(j):\left[\mathrm{Lw}_\phi^1(j),\mathrm{Lw}_\phi^2(j),\mathrm{Lw}_\phi^3(j)\right]. \tag{14}$$

For each curve with starting i point, its jitter component is extracted by

$$e_\phi(i)=\frac{2}{\mathrm{Sp}+1}\sum_{n=i}^{P_e(i)}|X_\phi(n)-\widehat{D}_\phi(n)|. \tag{15}$$

Then, the jitter components of the jth and $j-1$th curve of $\triangle(j)$ are expressed as

$$\mathrm{JV}_\phi(j):\left[e_\phi(i_j^F), e_\phi(i_{j-1}^F)\right]. \tag{16}$$

Finally, the big curve $c(j)$ can be converted as

$$\triangle(j):\{\mathrm{FS}_\phi(j),\mathrm{TR}_\phi(j),\mathrm{JV}_\phi(j)\}. \tag{17}$$

Therefore, through dividing the data curves and approximating the divided curves by fold line, the triangle can be used to describe the big curves. The main information, approximative fold lines including key point position $\mathrm{FS}_\phi(j)$, multiscale trends $\mathrm{TR}_\phi(j)$ of curves with different segments, and jitter components $\mathrm{JV}_\phi(j)$, are effectively extracted from the big curve $c(j)$ by STP.

Furthermore, the JSP is used to avoid the influence of amplitude and facilitate calculation. The extracted jitter components are used for jitter threshold of corresponding curve. The jitter threshold of the jth curve of starting with i_j^F point is shown below

$$\mathrm{Th}_\phi(j)=k*e_\phi\left(i_j^F\right). \tag{18}$$

Hence, the dynamic jitter threshold of three sides for triangle $\triangle(j)$ is expressed as

$$\mathrm{JT}_\phi(j):\left[\mathrm{Th}_\phi(i_j^F),\mathrm{Th}_\phi(i_{j-1}^F),\frac{\mathrm{Th}_\phi(i_j^F)+\mathrm{Th}_\phi(i_{j-1}^F)}{2}\right]. \tag{19}$$

Further, the trends $\mathrm{TR}_\phi(j)$ of triangle $\triangle(j)$ are signed

$$\widehat{\mathrm{Lw}}_\phi^1(j)=\begin{cases}1, & \mathrm{Lw}_\phi^1(j)>\mathrm{Th}_\phi(i_j^F)\\ 0, & |\mathrm{Lw}_\phi^1(j)|\le\mathrm{Th}_\phi(i_j^F)\\ -1, & \mathrm{Lw}_\phi^1(j)<-\mathrm{Th}_\phi(i_j^F)\end{cases} \tag{20}$$

$$\widehat{\mathrm{Lw}}_\phi^2(j)=\begin{cases}1, & \mathrm{Lw}_\phi^2(j)>\mathrm{Th}_\phi(i_{j-1}^F)\\ 0, & |\mathrm{Lw}_\phi^2(j)|\le\mathrm{Th}_\phi(i_{j-1}^F)\\ -1, & \mathrm{Lw}_\phi^2(j)<-\mathrm{Th}_\phi(i_{j-1}^F)\end{cases} \tag{21}$$

$$\widehat{\mathrm{Lw}}_\phi^3(j)=\begin{cases}1, & \mathrm{Lw}_\phi^3(j)>\frac{\mathrm{Th}_\phi(i_j^F)+\mathrm{Th}_\phi(i_{j-1}^F)}{2}\\ 0, & |\mathrm{Lw}_\phi^3(j)|\le\frac{\mathrm{Th}_\phi(i_j^F)+\mathrm{Th}_\phi(i_{j-1}^F)}{2}\\ -1, & \mathrm{Lw}_\phi^3(j)<-\frac{\mathrm{Th}_\phi(i_j^F)+\mathrm{Th}_\phi(i_{j-1}^F)}{2}.\end{cases} \tag{22}$$

When the trend change of curve is higher than the corresponding dynamic jitter threshold, the trend is signed as 1. When the trend change is lower than the corresponding negative jitter threshold, the trend is signed as -1. When the degree of the trend change is within dynamic jitter threshold, the trend is signed as 0. The signed trends $\widehat{\mathrm{TR}}_\phi(j)$ are expressed as

$$\widehat{\mathrm{TR}}_\phi(j):\left[\widehat{\mathrm{Lw}}_\phi^1(j),\widehat{\mathrm{Lw}}_\phi^2(j),\widehat{\mathrm{Lw}}_\phi^3(j)\right]. \tag{23}$$

Further, the center position $\overline{\mu}_\phi(j)$ of N_p' key points of ending with jth curve is calculated

$$\overline{\mu}_\phi(j)=\frac{1}{2^p+1}\sum_{n=j-2^p}^{j}\widehat{D}_\phi(i_n^E). \tag{24}$$

Then, the relative position between the end point of the jth curve and $\overline{\mu}_\phi(j)$ are calculated and signed by the jitter threshold

$$\beta_\phi(j)=\begin{cases}1, & \widehat{D}_\phi(i_j^E)-\overline{\mu}_\phi(j)>\mathrm{Th}_\phi(i_j^F)\\ \beta_\phi(j-1), & |\widehat{D}_\phi(i_j^E)-\overline{\mu}_\phi(j)|\le\mathrm{Th}_\phi(i_j^F)\\ -1, & \widehat{D}_\phi(i_j^E)-\overline{\mu}_\phi(j)<-\mathrm{Th}_\phi(i_j^F).\end{cases} \tag{25}$$

When the comparison of positions is higher than the jitter threshold, the end point of the jth is in the upper part of sine signal, and the sign is given as 1. When the comparison is lower than $-\mathrm{Th}_\phi(i_j^F)$, the end point of the jth is in the lower part of sine signal, and the sign is given as -1. When the difference degree is within the range of dynamic jitter threshold, position determination remains unchanged. Furthermore, the fault trend

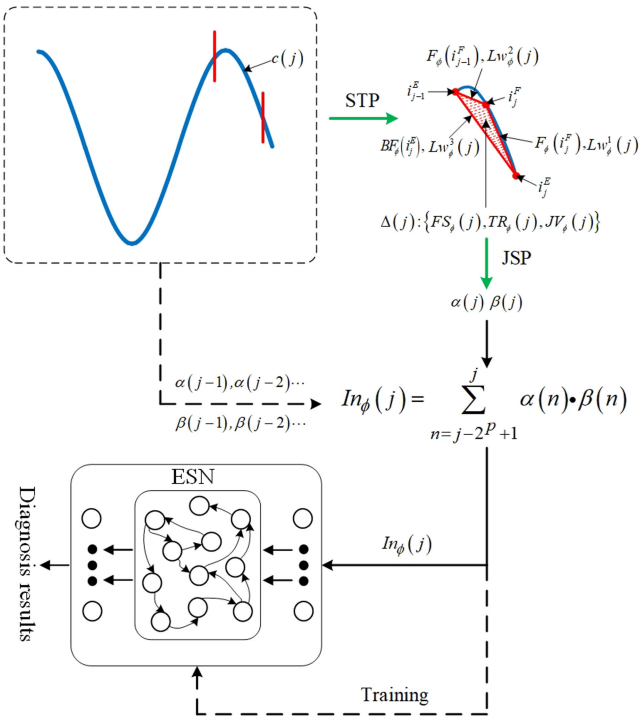

Fig. 5. Overall principle diagram of the proposed algorithm.

$\alpha_\phi(j)$ is obtained by

$$\alpha_\phi(j) = \left(1-|\widehat{\mathrm{Lw}}_\phi^1(j)|\right) \wedge \left(1-|\widehat{\mathrm{Lw}}_\phi^2(j)|\right) \wedge \left(1-|\widehat{\mathrm{Lw}}_\phi^3(j)|\right) \tag{26}$$

where $|\cdot|$ is absolute operation, $\wedge$ is logic union processing. Then, the quantitative trend fault degree $\mathrm{In}_\phi(j)$ is obtained by

$$\mathrm{In}_\phi(j) = \sum_{n=j-2^p+1}^{j} \alpha_\phi(n) \cdot \beta_\phi(n). \tag{27}$$

The variable $\mathrm{In}_\phi(j)$ is an integer variable. Every change is quantitative, which is either quantitative 1 or unchanged. It can effectively reduce the fluctuation and quantity of fault data features. Meanwhile, only one variable contains fault degree and location information. These characteristics are very conducive to the training of data and the stability of diagnostic results.

Finally, ESN [28]–[31] is used to implement the classification of fault data. The ESN is a new recurrent neural network with high generalization capability and short training period, which improve many problems of traditional neural network (NNs) such as local minima, overtraining, and high computational burden [28]–[31]. For ESN, it uses an interconnected recurrent grid of processing neurons called dynamical reservoir to replace the hidden layer of NNs. Only the output weights need to be trained, while the reservoir weights and input weights usually are given randomly. Meanwhile, simple linear regression is used to train the network [30]–[31]. These features can make the training speed of the whole network very fast; the structure designing and debugging are also more convenient. The mathematical details of ESN can be found in [28] and [29]. The overall principle diagram of the proposed algorithm is shown in Fig. 5.

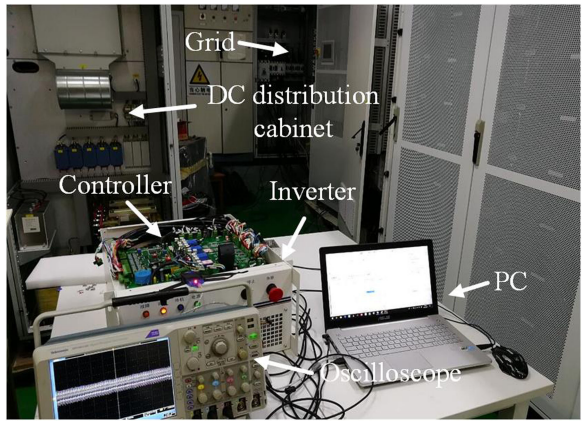

Fig. 6. Experiment platform.

III. Experiment Evaluation

Experiments are carried out to verify the effectiveness of the proposed method. The experimental platform is shown in Fig. 6. The system is controlled by TMS320F28335PGFA. Microgrid inverter uses a 20-kW inverter of three phases with six insulated gate bipolar transistor (IGBT) switches. DC cabinet provides 600-V dc-link voltage. The frequency of inverter is 50 Hz. Sampling frequency is set to 10 kHz. Filter inductance and capacitance are 1 mH and 50 μF, respectively. For the proposed algorithm, p takes 3, then N_p' is 9, N_c' is 8. The obtained variables In_a, In_b, and In_c are used for the input of ESN. The number of input layer takes 3. The reserve pool is set as 40. The number of output layer is 6, which represents the diagnosis results of 6 switches.

Fig. 7 shows the diagnosis results and intermediate variables of the proposed fault diagnosis algorithm under s1 open-circuit fault with the unbalanced state. In Fig. 7(a), it can be seen that the phase A is unbalanced with phases B and C. Fig. 7(b) shows the dynamic jitter thresholds. From the experimental results, it can be understood that the dynamic jitter thresholds of different curves of three-phase currents are effectively extracted. In Fig. 7(c) the quantitative trend fault degrees of three-phase currents are stable and does no change in normal state. When the s1 fault occurs, it is quantitatively changed, which are not affected by the unbalance component. Fig. 7(d) shows the diagnosis results. From the experimental results, it can be seen that when the inverter is in unbalanced state, it does not cause false alarm; meanwhile, when s1 fault occurs, it is accurately diagnosed. In addition, the diagnosis features and result are stable. Hence, it can be seen that the proposed algorithm not only can identify inverter fault but also has better robustness to unbalanced state.

Fig. 8 shows the fault diagnosis results and intermediate variables of the proposed fault diagnosis algorithm under s1 and s3 open-circuit faults with overcurrent component interference. In Fig. 8(a), when the inverter is in normal state, the three-phase currents are symmetric. When s1 and s3 open-circuit faults occur, the phase A and phase B lose symmetry. Phase C has an overcurrent component. It is obvious that the phase C also loses the symmetry, which is a kind of overcurrent component

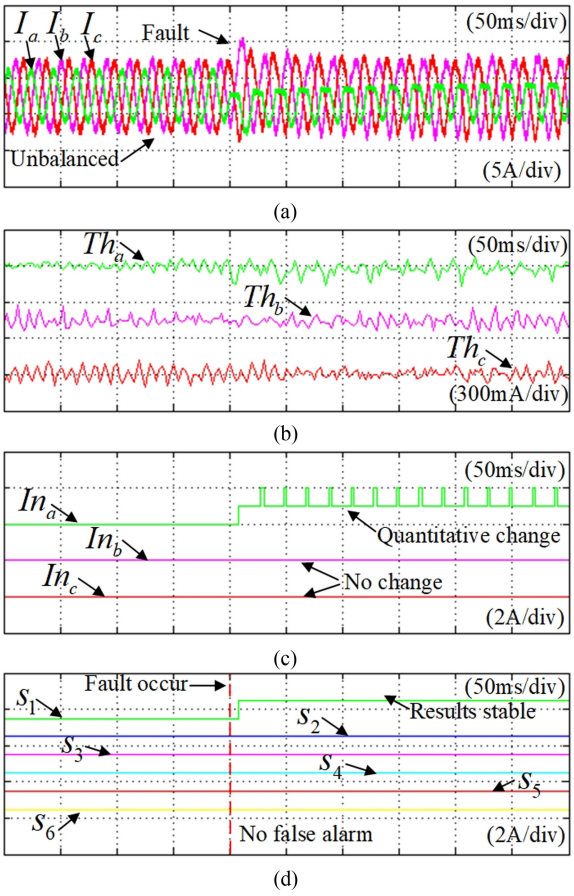

Fig. 7. s1 fault with single-phase unbalanced state. (a) Three-phase currents. (b) Dynamic jitter thresholds. (c) Quantitative trend fault degree. (d) Diagnosis results.

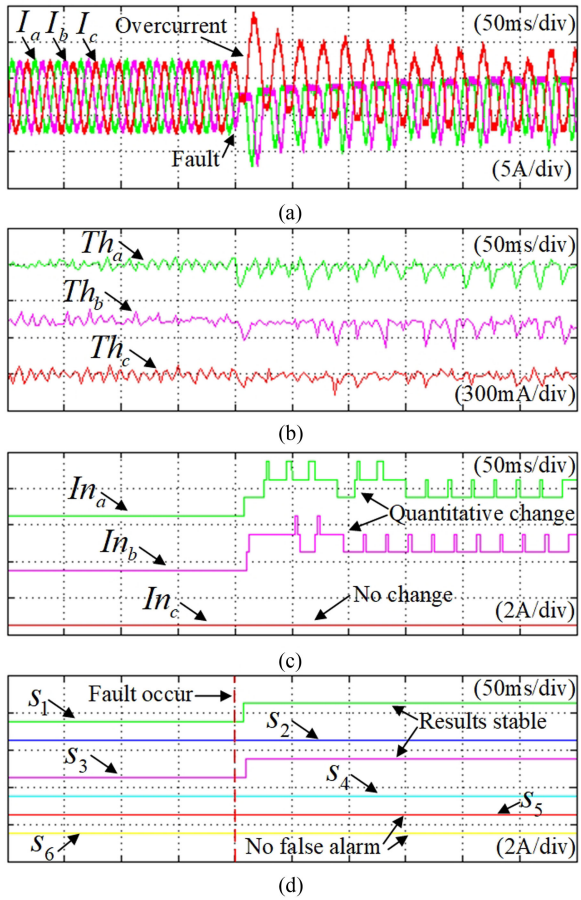

Fig. 8. s1 and s3 faults with overcurrent component interference. (a) Three-phase currents. (b) Dynamic jitter thresholds. (c) Quantitative trend fault degree. (d) Diagnosis results.

intermediate. In Fig. 8(b), it can be seen that the dynamic jitter thresholds of different curves of three-phase currents are effectively extracted. Fig. 8(c) shows the quantitative trend fault degree; it can be seen that when the inverter output is in normal state, the variables In_a, In_b, and In_c do not change. When s1 and s3 fault occur, the quantitative trend fault degree In_a and In_b of phase A and phase B quantificationally change, which is either quantitative 1 or unchanged. Meanwhile, the variable is larger than 0, which indicates the failure of the upper switch. It is to say that the quantitative trend fault degree also includes the position information. In addition, it is obvious that In_c is always unchangeable when the overcurrent occurs, which can effectively shield the overcurrent component interference. In Fig. 8(d), s1 and s3 faults are diagnosed. Meanwhile, s5 and s6 of phase C do not appear false alarm caused by overcurrent.

Fig. 9 shows the fault diagnosis results and intermediate variables of the proposed fault diagnosis algorithm under s1 open-circuit fault with multiphase unbalanced state. In Fig. 9(a), when the inverter is in normal state, the three-phase currents A, B, and C are unbalanced. When s1 open-circuit fault occurs, three-phase currents have some distortion, and the phase A loses part periodic signal. In Fig. 9(b), it can be seen that the dynamic jitter thresholds of different curves of three-phase currents are also effectively extracted in this case. In Fig. 9(c), quantitative trend fault degree is shown; it is obvious that when the inverter output is in normal state with multiphase unbalanced state, the variables In_a, In_b, and In_c do not change. When s1 fault occurs, corresponding In_a of phase A quantificationally changes, which is either quantitative 1 or unchanged. Meanwhile, In_b and In_c are always unchangeable when the s1 fault occurs. In Fig. 9(d), s1 fault is diagnosed. Meanwhile, s2, s3, s4, s5, and s6 of phase B and phase C do not appear false alarm caused by multiphase unbalanced state.

Fig. 10 shows the diagnosis results and intermediate variables of the proposed fault diagnosis algorithm under multiswitch s1 and s4 open-circuit faults. In Fig. 10(a), it can be seen that when the s1 and s4 open-circuit faults occur, the symmetry of the corresponding phases A and B are lost. Fig. 10(b) shows the dynamic jitter thresholds. From the experimental results, it can be understood that the dynamic jitter thresholds of different curves of three-phase currents are effectively extracted. In Fig. 10(c), when inverter is in normal state, the quantitative trend fault degrees of three-phase currents are stable and no change occurs. When the s1 and s4 faults occur, corresponding variables

TABLE I
COMPARISON OF FAULT DIAGNOSIS PERFORMANCE BETWEEN EXITING ALGORITHMS AND PROPOSED ALGORITHM

Relevant research algorithms	Whether consider condition1	Whether consider condition2	Fault feature extraction	Dependence of system model	Dependence of weights or thresholds	Startup of algorithm per cycle	Diagnosis speed of algorithm	Detection signals
[26]	no	no	CD	high	high	-	$< 1T$	current, voltage
[27]	no	no	CD	high	high	40	$< 0.2T$	current, voltage
[10]	no	no	CD	high	high	-	about $0.5T$	current
[12]	no	no	CD	high	high	-	about $0.25T$	current
[14]	no	no	AF	low	high	200	about $0.25T$	current
[17]	no	no	AF	low	high	-	about $0.385T$	current
Proposed	yes	yes	MTF	low	low	8	about $0.3T$	current

Condition 1: unbalanced state.
Condition 2: overcurrent component interference.
CD refers comparison difference with variable expectation, observer, or model. AF refers asymmetric feature of data.
MTF refers multiscale trend features of data.

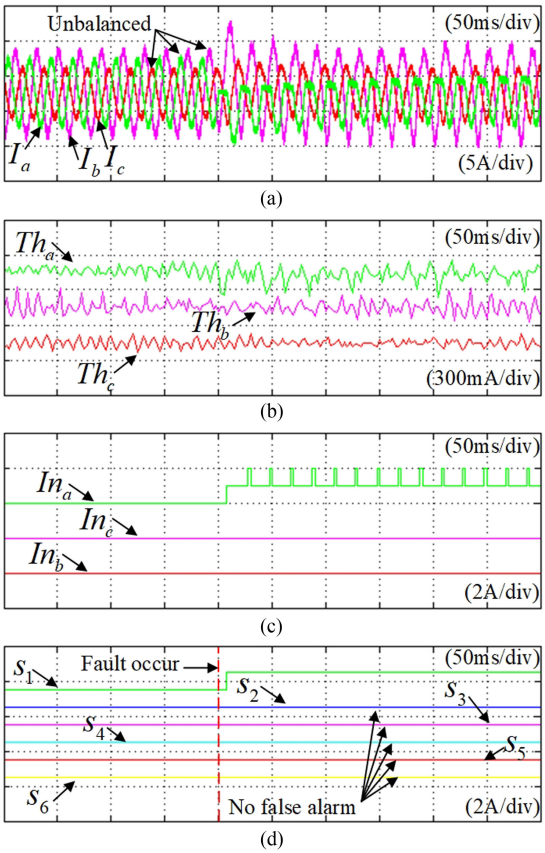

Fig. 9. s1 fault with multiphase unbalanced state. (a) Three-phase currents. (b) Dynamic jitter thresholds. (c) Quantitative trend fault degree. (d) Diagnosis results.

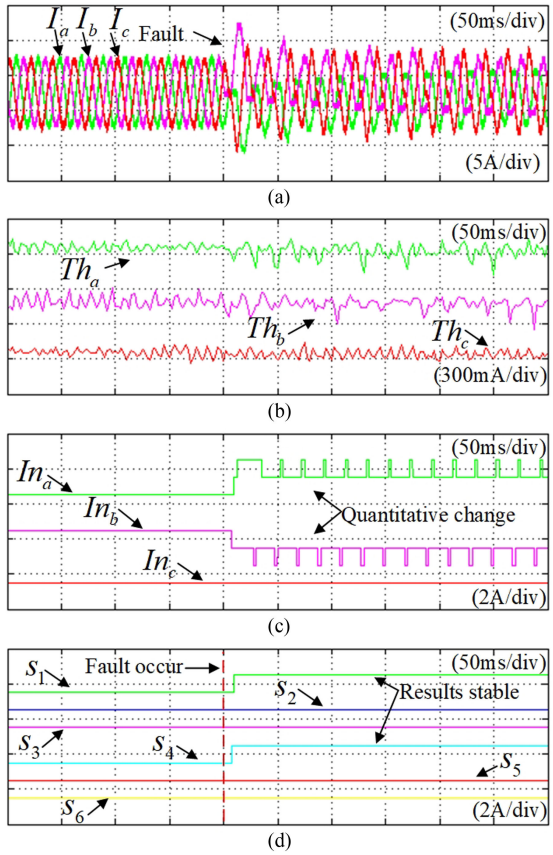

Fig. 10. Multiswitch s1 and s4 open-circuit faults. (a) Three-phase currents. (b) Dynamic jitter thresholds. (c) Quantitative trend fault degree. (d) Diagnosis results.

In_a and In_b are quantitatively changed; meanwhile, the variable In_c is not affected. Fig. 10(d) shows the diagnosis results; it can be seen that when s1 and s4 faults occur, they are diagnosed.

In order to further demonstrate the performance of the proposed fault diagnosis algorithm, the related comparisons and summaries have been made with some relevant existing methods from several performance aspects in Table I. For the research conditions, although Condition 1 and 2 have great influences on inverter fault diagnosis, these conditions are neglected in many existing inverter fault diagnosis algorithms, e.g., [10], [12], [14], [17], [26], [27], and so on. However, the proposed fault diagnosis algorithm considers both Condition 1 and 2 in this article, which can effectively improve the robustness of the algorithm.

For fault feature extraction, CD and AF are common methods of fault feature extraction for inverter. However, compared with them, MTF method is used to extract fault feature in this article, which can effectively reduce the influence of unbalanced state and overcurrent component interference. Meanwhile, it also has low dependence of system model. On the other hand, compared

with [10], [12], [14], [17], [26], and [27], the proposed fault diagnosis algorithm uses ESN and JSP based on the jitter component, which leads to the low dependence of weights or thresholds. Another point to be noted is that, because the proposed fault diagnosis algorithm is driven by the slidable triangular and p takes 3 in this article, the startup is 8 times per cycle. For the diagnosis speed, the highest diagnosis speed of the proposed fault diagnosis algorithm is about 0.3T, which is within a reasonable range. Meanwhile, it is also better than existing methods, e.g. [10], [17], and [26].

Furthermore, through above experiments and comparisons, the main performance of the proposed fault diagnosis algorithm are summarized as follows. The proposed fault diagnosis algorithm has better robustness to unbalanced state and overcurrent component interference. From the diagnosis results of Figs. 7(d), 8(d), and 9(d), it can be seen that under the case of unbalanced state or overcurrent component interference, the diagnosis results of the proposed fault diagnosis algorithm do not appear false alarm. The proposed fault diagnosis algorithm has low startup times. Because the fault diagnosis algorithm is driven by the slidable triangular, it can reduce the startup times. Because p takes 3, the startup is 8 times per cycle. Because of the use of ESN, the proposed fault diagnosis algorithm has low dependence of system model, weights, or thresholds. ESN is based on data fitting, which avoids the setting and selecting of the diagnosis thresholds of multiswitches fault diagnosis. In addition, because of the structure features of ESN, the adjustment of hidden layer node parameters is also avoided. The feature variable of quantitative trend fault degree reduces the training burden and the number of input features of network training. From Figs. 7(c), 8(c), 9(c), and 10(c), it can be seen that the variable In_{ϕ} is an integer variable. Every change is quantitative, which is either quantitative 1 or unchanged. This feature can effectively reduce the fluctuation and quantity of fault data features. In addition, only one variable contains fault degree and location information, which also reduces unnecessary input of features.

IV. Conclusion

A multiswitch open-circuit fault diagnosis algorithm of microgrid inverter based on STP has been proposed. Compared with the existing fault diagnosis algorithms, it has better robustness to unbalanced state and overcurrent component interference. These features make it more suitable under microgrid environment. In that, the STP is used to extract the key features and reduce the startup times of algorithm. Then, the JSP is used to reduce the influence of amplitude and facilitate calculation. Further, the quantitative trend fault degree is calculated to reflect the degree of trend fault and fault position information. Finally, the ESN is used to detect the type and the location of the inverter switch fault, which makes the design, implementation, and debugging of fault diagnosis more convenient. The related experimental results have been given to demonstrate the effectiveness of the proposed algorithm.

References

[1] M. Zolfaghari, S. H. Hosseinian, S. H. Fathi, M. Abedi, and G. B. Gharehpetian, "A new power management scheme for parallel-connected PV systems in microgrids," *IEEE Trans. Sustain. Energy*, vol. 9, no. 4, pp. 1605–1617, Oct. 2018.

[2] Y. Zhu, Q. Fan, B. Liu, and T. Wang, "An enhanced virtual impedance optimization method for reactive power sharing in microgrids," *IEEE Trans. Power Electron.*, vol. 33, no. 12, pp. 10390–10402, Dec. 2018.

[3] Q. Sun, S. Chen, L. Chen, and D. Ma, "Quasi-Z-source network-based hybrid power supply system for aluminum electrolysis industry," *IEEE Trans. Ind. Inform.*, vol. 13, no. 3, pp. 1141–1151, Jun. 2017.

[4] S. Mahmoud and U. Rahman, "Networked control approach for distributed generation systems," *IEEE/CAA J. Automatica Sinica*, vol. 5, no. 4, pp. 836–851, Jul. 2018.

[5] F. Nejabatkhah, Y. W. Li, K. Sun, and R. Zhang, "Active power oscillation cancellation with peak current sharing in parallel interfacing converters under unbalanced voltage," *IEEE Trans. Power Electron.*, vol. 33, no. 12, pp. 10200–10214, Dec. 2018.

[6] Y. Xia, W. Wei, M. Yu, Y. Peng, and J. Tang, "Decentralized multitime scale power control for a hybrid AC/DC microgrid with multiple subgrids," *IEEE Trans. Power Electron.*, vol. 33, no. 5, pp. 4061–4072, May 2018.

[7] X. Sun, Y. Hao, Q. Wu, X. Guo, and B. Wang, "A multifunctional and wireless droop control for distributed energy storage units in islanded AC microgrid applications," *IEEE Trans. Power Electron.*, vol. 32, no. 1, pp. 736–751, Jan. 2017.

[8] Z. Jin, L. Meng, J. M. Guerrero, and R. Han, "Hierarchical control design for shipboard power system with DC distribution and energy storage aboard future more-electric ships," *IEEE Trans. Ind. Inform.*, vol. 14, no. 2, pp. 703–714, Feb. 2018.

[9] J. Poon, P. Jain, I. C. Konstantakopoulos, C. Spanos, S. K. Panda, and S. R. Sanders, "Model-based fault detection and identification for switching power converters," *IEEE Trans. Power Electron.*, vol. 32, no. 2, pp. 1419–1430, Feb. 2017.

[10] X. Wu, R. Tian, S. Cheng, T. Chen, and L. Tong, "A non-intrusive diagnostic method for open-circuit faults of locomotive inverters based on output current trajectory," *IEEE Trans. Power Electron.*, vol. 33, no. 5, pp. 4328–4341, May 2018.

[11] S. M. Jung, J. S. Park, H. W. Kim, K. Y. Cho, and M. J. Youn, "An MRAS-based diagnosis of open-circuit fault in PWM voltage-source inverters for PM synchronous motor drive systems," *IEEE Trans. Power Electron.*, vol. 28, no. 5, pp. 2514–2526, May 2013.

[12] Q. T. An, L. Sun, and L. Z. Sun, "Current residual vector-based open switch fault diagnosis of inverters in PMSM drive systems," *IEEE Trans. Power Electron.*, vol. 30, no. 5, pp. 2814–2827, May 2015.

[13] M. A. Freire, J. O. Estima, and J. M. Cardoso, "A new approach for current sensor fault diagnosis in PMSG drives for wind energy conversion systems," *IEEE Trans. Ind. Appl.*, vol. 50, no. 2, pp. 1206–1214, Apr. 2014.

[14] F. Wu and J. Zhao, "A real-time multiple open-circuit fault diagnosis method in voltage-source-inverter fed vector controlled drives," *IEEE Trans. Power Electron.*, vol. 31, no. 2, pp. 1425–1437, Feb. 2016.

[15] J. O. Estima and A. J. M. Cardoso, "A new approach for real-time multiple open-circuit fault diagnosis in voltage-source inverters," *IEEE Trans. Ind. Appl.*, vol. 47, no. 6, pp. 2487–2494, Nov./Dec. 2011.

[16] H. Zhao and L. Cheng, "Open switch fault diagnostic method for back to back converters of doubly fed wind power generation system," *IEEE Trans. Power Electron.*, vol. 33, no. 4, pp. 3452–3461, Apr. 2018.

[17] H. Wei *et al.*, "A new diagnostic algorithm for multiple IGBTs open circuit faults by the phase currents for power inverter in electric vehicles," *Energies*, vol. 11, no. 6, pp. 1508–1521, Apr. 2018.

[18] I. Jlassi, J. O. Estima, S. K. El Khil, N. M. Bellaaj, and A. J. M. Cardoso, "Multiple open-circuit faults diagnosis in back-to-back converters of PMSG drives for wind turbine systems," *IEEE Trans. Power Electron.*, vol. 30, no. 5, pp. 2689–2702, May 2015.

[19] R. Selvaraj, K. Desingu, T. R. Chelliah, D. Khare, and C. Bharatiraja, "Fault tolerant operation of parallel-connected 3L-neutral-point clamped back-to-back converters serving to large hydro-generating units," *IEEE Trans. Ind. Appl.*, vol. 54, no. 5, pp. 5429–5443, Oct. 2018.

[20] M. S. Golsorkhi and D. C. Lu, "A decentralized control method for islanded microgrids under unbalanced conditions," *IEEE Trans. Power Del.*, vol. 31, no. 3, pp. 1112–1121, Jun. 2016.

[21] K. Sun, X. Wang, Y. W. Li, F. Nejabatkhah, Y. Mei, and X. Lu, "Parallel operation of bidirectional interfacing converters in a hybrid AC/DC microgrid under unbalanced grid voltage conditions," *IEEE Trans. Power Electron.*, vol. 32, no. 3, pp. 1872–1884, Mar. 2017.
[22] F. Nejabatkhah, Y. W. Li, and K. Sun, "Parallel three-phase interfacing converters operation under unbalanced voltage in hybrid AC/DC microgrid," *IEEE Trans. Smart Grid*, vol. 9, no. 2, pp. 61310–1322, Mar. 2018.
[23] A. H. Etemadi and R. Iravani, "Overcurrent and overload protection of directly voltage-controlled distributed resources in a microgrid," *IEEE Trans. Ind. Electron.*, vol. 60, no. 12, pp. 5629–5638, Dec. 2013.
[24] N. Hatziargyriou, "Microgrid protection," in *Microgrids: Architectures and Control*. Piscataway, NJ, USA: Wiley-IEEE Press, 2014, pp. 117–164.
[25] X. Xu, J. Mitra, T. Wang, and L. Mu, "An evaluation strategy for microgrid reliability considering the effects of protection system," *IEEE Trans. Power Del.*, vol. 31, no. 5, pp. 1989–1997, Oct. 2016.
[26] J. Lamb and B. Mirafzal, "Open-circuit IGBT fault detection and location isolation for cascaded multilevel converters," *IEEE Trans. Ind. Electron.*, vol. 64, no. 6, pp. 4846–4856, Jun. 2017.
[27] S. Yang, Y. Tang, and P. Wang, "Seamless fault-tolerant operation of a modular multilevel converter with switch open-circuit fault diagnosis in a distributed control architecture," *IEEE Trans. Power Electron.*, vol. 33, no. 8, pp. 7058–7070, Aug. 2018.
[28] H. Jaeger and H. Haas, "Harnessing nonlinearity: Predicting chaotic systems and saving energy in wireless communication," *Sci.*, vol. 304, no. 5667, pp. 78–80, Apr. 2004.
[29] S. Lokse, F. Bianchi, and R. Jenssen, "Training echo state networks with regularization through dimensionality reduction," *Cognit. Comput.*, vol. 9, no. 3, pp. 364–378, Jun. 2017.
[30] X. Yao, Z. Wang, and H. Zhang, "A novel photovoltaic power forecasting model based on echo state network," *Neurocomputing*, to be published, doi: 10.1016/j.neucom.2018.10.022.
[31] X. Yao, Z. Wang, and H. Zhang, "Identification method for a class of periodic discrete-time dynamic nonlinear systems based on sinusoidal ESN," *Neurocomputing*, vol. 275, pp. 1511–1521, Jan. 2018.

Zhanjun Huang was born in Shandong, China, in 1989. He received the M.S. degree in electrical theory and new technology and Ph.D. degree in power electronics and power transmission from Northeastern University, Shenyang, China, in 2014 and 2019, respectively.

He is currently an Associate Professor with the Northwestern Polytechnical University, Xian, China. His current research interests include data processing and analysis, machine learning, neural networks, fault diagnosis, health management, and their applications in power electronics.

Zhanshan Wang (Senior Member, IEEE) was born in Liaoning, China, in 1971. He received the M.S. degree in control theory and control engineering from Fushun Petroleum Institute (now Liaoning Shihua University), Fushun, China, in 2001, and the Ph.D. degree in control theory and control engineering from the Northeastern University, Shenyang, China, in 2006.

Since 2010, he has been a Professor with Northeastern University. He has authored and coauthored over 110 journal and conference papers and five monographs. He is also the holder of ten patents. His research interests include the stability analysis of recurrent neural networks, fault diagnosis, fault tolerant control, nonlinear control theory, and their applications in smart grid.

Dr. Wang was an Associate Editor for IEEE TRANSACTION ON NEURAL NETWORKS AND LEARNING SYSTEMS. He is also a member of Editorial Board of *Acta Automatica Sinica*.